Production and characterization of spiral phase plates for optical wavelengths

S. S. R. Oemrawsingh, J. A. W. van Houwelingen, E. R. Eliel, J. P. Woerdman, E. J. K. Verstegen, J. G. Kloosterboer, and G. W. 't Hooft

We describe the fabrication and characterization of a high-quality spiral phase plate as a device to generate optical vortices of low (3–5) specified charge at visible wavelengths. The manufacturing process is based on a molding technique and allows for the production of high-precision, smooth spiral phase plates as well as for their replication. An attractive feature of this process is that it permits the fabrication of nominally identical spiral phase plates made from different materials and thus yielding different vortex charges. When such a plate is inserted in the waist of a fundamental Gaussian beam, the resultant far-field intensity profile shows a rich vortex structure, in excellent agreement with diffraction calculations based on ideal spiral phase plates. Using a simple optical test, we show that the reproducibility of the manufacturing process is excellent. © 2004 Optical Society of America

OCIS codes: 050.1970, 220.4000, 220.4610.

1. Introduction

Optical waves that possess a helical phase distribution have been addressed in many studies,[1–3] with applications in the cooling and trapping of neutral atoms,[4] Bose–Einstein condensates,[5] the generation of vortex solitons, and the manipulation of small macroscopic particles.[6,7] The helical phase distribution implies the presence of a phase singularity, also called an optical vortex, and is characterized by a locally vanishing intensity. In the vicinity of such a vortex, the complex field amplitude depends locally on azimuthal angle θ through

$$u(\rho, \theta, z) = u'(\rho, z)\exp(iQ\theta), \tag{1}$$

where u' can be a complex function, ρ is the radial coordinate, and z is the coordinate in the direction of propagation. Following a closed path about the vortex, the topological charge of the vortex is defined as[8]

$$Q = \frac{1}{2\pi} \oint \mathrm{d}\chi, \tag{2}$$

where χ is the phase of the field. In most studies that involve optical vortex fields, an optical beam in a cylindrically symmetric mode with a vortex in its center is used. This is also the simplest example of such a field and as such is fully described by Eq. (1).

Because photons in a mode of topological charge Q carry orbital angular momentum with expectation value $Q\hbar$,[9] photons in helical modes have recently attracted considerable attention. Issues that have been studied include conservation and entanglement of photonic orbital angular momentum in spontaneous parametric downconversion.[10–16] The interest in the latter stems from the fact that a helical photon represents a high-dimensional quantum system, thus permitting the construction of high-dimensional alphabets for quantum information.[11]

One can generate optical vortex beams quite easily by sending a higher-order Hermite–Gaussian laser beam through a combination of cylindrical lenses[1] or by diffracting a nonhelical laser beam off a computer-generated hologram that itself carries a vortex.[17–19] The latter method enjoys considerable popularity because such holograms are quite easy to fabricate. Another approach to the generation of vortex beams

S. S. R. Oemrawsingh (soemraws@molphys.leidenuniv.nl), J. A. van Houwelingen, E. R. Eliel, and J. P. Woerdman are with the Huygens Laboratory, Leiden University, P.O. Box 9504, 2300 RA Leiden, The Netherlands. E. J. K. Verstegen, J. G. Kloosterboer, and G. W. 't Hooft are with the Philips Research Laboratories, Prof. Holstlaan 4, 5656 AA Eindhoven, The Netherlands.

Received 22 July 2003; revised manuscript received 1 October 2003; accepted 15 October 2003.

0003-6935/04/030688-07$15.00/0

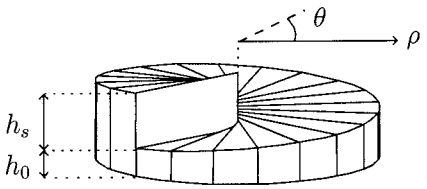

Fig. 1. Sketch of the spiral phase plate. The top surface spirals upward from height h_0 to $h_0 + h_s$.

involves the use of a spiral phase plate[9,20] (SPP), which is the subject of the present paper.

2. Spiral Phase Plates

A SPP is an optical element that imposes an azimuth-dependent retardation on the optical field. In its simplest form, as shown in Fig. 1, it is a transparent plate of refractive index n whose height is proportional to azimuthal angle θ:

$$h = h_s \frac{\theta}{2\pi} + h_0, \tag{3}$$

where h_s is the step height and h_0 is the base height of the device. This configuration yields an azimuth-dependent optical phase delay:

$$\phi(\theta, \lambda) = \frac{2\pi}{\lambda}\left[\frac{(n - n_0)h_s\theta}{2\pi} + nh_0\right], \tag{4}$$

where n_0 is the refractive index of the surrounding medium. When such a plate is inserted in the waist of a Gaussian beam, where the phase distribution is plane, it imprints a vortex with a charge equal to $Q = h_s(n - n_0)/\lambda$, thereby generating an output beam that carries orbital angular momentum per photon equal to $Q\hbar$. Note here that the value of Q depends both explicitly and implicitly (through the refractive index) on the wavelength of the incident light, betraying the chromatic nature of this device. The resultant phase distribution is illustrated in Fig. 2.

To obtain a device that is able to generate beams with low values of Q, it is clear that step height h_s of the plate should be of the order of the wavelength, λ. Alternatively, the SPP can be made to be almost index matched to its surroundings, $\Delta n = |n - n_0| \approx 0$.

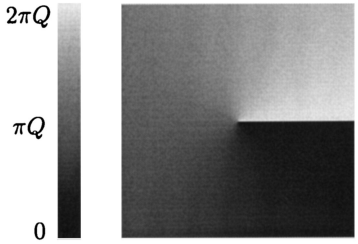

Fig. 2. Phase distribution imprinted onto the transverse plane of an incident beam. When Q is an integer number, the phase change at the transition from black to white is actually smooth. Otherwise, the sharp transition in gray level represents a phase discontinuity.

This approach was followed in the original work on spiral phase plates for use in the optical regime as reported by Beijersbergen *et al.*,[9] for which $h_s \approx 0.7$ mm and $\Delta n \approx 9 \times 10^{-4}$. They achieved index matching by immersing the SPP in a liquid whose refractive index they controlled by tuning the temperature. Density variations in the liquid were a major problem in that experiment. A more extreme example of this index-matching technique is provided by the recently developed SPP in the x-ray regime[20] for which $\Delta n \approx 4 \times 10^{-6}$. Here, index matching occurs naturally.

Apart from issues related to index matching, the difficulties of manufacturing a SPP center on (i) the steepness of the step, (ii) the central part of the SPP where, ideally, the height spirals up in a region with zero diameter, and (iii) the smoothness of the ramp. Indeed, the SPPs in the visible[9] and x-ray[20] regions did not have a smooth ramp but were staircaselike. Only the first SPP ever reported had a smooth structure, but it was used at wavelengths far from the optical regime (10 μm).[21]

Here, we report on a novel technique for manufacturing SPPs for optical wavelengths based on state-of-the-art micromachining and molding. Our technique is based on technologies originally developed at Philips Research Laboratories for the mass fabrication of lightweight aspheres for the optical pick-up units of CD players.[22] In our case, it permits the fabrication of multiple SPPs by replication from a master.

3. Production

The manufacturing technique is based on crafting a mold that, naturally, is the negative of the SPP that we wish to produce. The mold is machined with a diamond tool in a piece of brass by use of a modified version of the COLATH, a high-precision computer-driven lathe.[23] This lathe can be programmed to produce the surface that we require.

Postfabrication inspection of the mold is made with a high-accuracy interferometric metrology system (Zygo); typical results are shown in Fig. 3. The two parts of the figure demonstrate the depth variations along a radial and along an azimuthal path across the mold. These measurements yielded a value of the step height equal to 5.07 μm (design value, 5.00 μm), a linear relation between local depth h and the azimuthal angle with a rms deviation of order 15 nm, and an azimuthal width of the step discontinuity of ~6°. Along a radial path of 4.2-mm length, the depth can be seen to increase by ≈150 nm. Note that the mold thus deviates from its design by much less than half of an optical wavelength in the visible regime. Naturally, in the central part where the height anomaly resides, the deviations were larger, owing to technological difficulties. The diameter of this anomaly in the mold was measured to be ~50 μm, very small compared to the overall diameter of the device (8.4 mm).

The mold is then used for the production of the SPPs, as shown in Fig. 4. It is first treated with

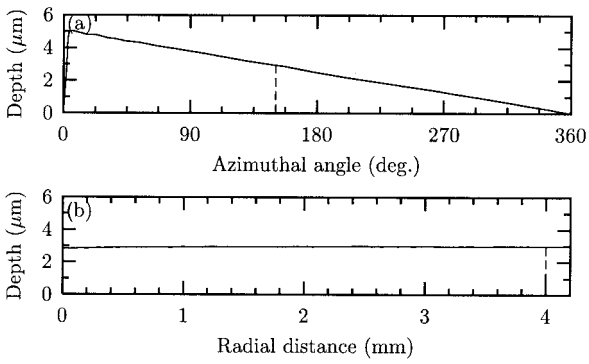

Fig. 3. These figures, based on high-accuracy data from the Zygo interferometric metrology system, demonstrate the quality of the mold. (a) The depth of the mold is plotted following an azimuthal path with a radius of ≈4 mm, revealing a smooth ramp. The steepness of the step can also be seen clearly. There the mold's depth increases from 0 to 5.07 μm over an azimuthal range of ~6°. The vertical, dashed line indicates the position at which the bottom figure was measured. (b) Depth of the mold plotted along a radial path at an azimuthal angle ≈151°. The deviation from the expected horizontal line is ~150 nm, which is considerably smaller than the optical wavelength at which the device is designed to work (813 nm). The vertical, dashed line indicates the position at which the top figure was measured.

stearic acid, thereby generating an antistick layer. Then a 50-μm-thick ring-shaped spacer is placed about the mold, whereupon a monomer of poly(ethylene glycol) dimethacrylate is cast into the mold. A cover-glass plate, which has been treated with [γ-(methacryloxyloxy)propyl]trimethoxysilane to allow the polymer to attach to it, is then pressed onto the spacer, pushing out the excess monomer. Subsequently, the monomer is cured by use of UV radiation from an EFOS Acticure 4000 (EXFO, Vanier, Quebec, Canada) equipped with a high-pressure mercury lamp, a fiber-optic waveguide, and a filter with a transmission band of 320–390 nm. Curing takes 100 s at an intensity of 40 mW/cm^2, during which full conversion to a polymer is achieved. The usual curing requirement of a low-oxygen environment does not apply here because the monomer is

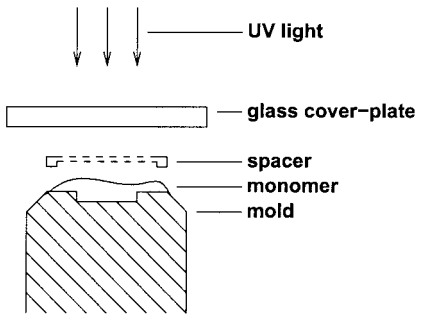

Fig. 4. Schematic overview of the production of a spiral phase plate. The monomer is cast into the mold, and a spacer is placed around it. A glass cover plate is pressed against the monomer and onto the spacer, after which the monomer is cured by illumination by UV light to a cross-linked polymer network.

sandwiched between cover plate and mold and because it is exposed to high-intensity radiation. During the polymerization process the material usually shrinks (typical shrinkage in polymer molding technology is roughly 3%). After release of the plate from the mold we obtained a solid SPP with base height $h_0 \approx 50$ μm, step height $h_s \approx 5$ μm, and a refractive index at 632.8 nm of 1.495 firmly attached to a glass substrate. Naturally, any other polymer that possesses a different refractive index can be used and will yield a SPP that is capable of generating a different vorticity at the same design wavelength.

4. Characterization of the Spiral Phase Plate

Both the quality of the molded SPP and its transmission properties have been studied by a variety of optical methods.

An inspection of the device with the naked eye reveals that the surface is smooth and that the step and the central part where the height anomaly lies are hardly visible. No air bubbles appear to be present inside the polymer, nor can an air layer be seen between the glass and polymer (it would betray itself by exhibiting Newton rings).

A. Reflection Study

For a microscopic study of the surface we used a phase-contrast microscope and illuminated the SPP from the top with an incandescent lamp and an interference filter ($\lambda = 549$ nm, $\Delta\lambda \approx 10$ nm), thus looking at reflected light. This method causes height variations to appear as interference fringes. We observed that the angular spacing of the interference fringes over the SPP was constant [see Fig. 5(a)], implying that the device's azimuthal ramp is linear, as designed [cf. Eq. (3)] and as is more clearly demonstrated in Fig. 6, where the fringes have been translated into height variations and plotted against their azimuthal positions. From these data we found step height h_s to be $\approx 5.05 \pm 0.07$ μm. This measurement implies, surprisingly, that the polymer has shrunk either not at all or very little, but at any rate much less than the value of 3% that is assumed to be typical.

To study the step discontinuity of the SPP we looked at it far away from the center, as shown in Fig. 5(b), in which a fringe pattern with an angular width of 6° whose height changes rapidly is shown.

The area where the interference pattern is irregular corresponds to the imperfect center of the device, i.e., the region of the height anomaly. The anomaly can be seen clearly in the close-up [Fig. 5(c)] and has approximately the same size as in the mold (≈50 μm). The error caused by this region of uncontrolled height is expected to be small as long as the width of an incident beam is much greater than 50 μm.

B. Transmission Study

The vorticity imprinted on a fundamental Gaussian beam is not apparent in the intensity distribution in the near field of the imprinting device. This is so because, although the beam has been phase shifted,

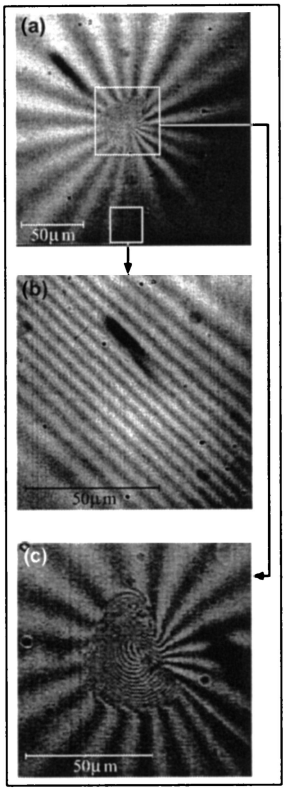

Fig. 5. CCD images captured with a phase-contrast microscope that is looking at light (wavelength, 549 nm) reflected off the surface of a spiral phase plate, produced with the mold shown in Fig. 3. (a) The fringe spacing remains constant over the angular direction of the plate. The center is dominated by the finite size of the height anomaly. (b) Close-up of the step located in the region indicated by the box at the bottom of (a). In reality, the part of the step that is shown in (b) lies much farther away from the center of the device. The step has an angular width of ~6°. (c) Close-up of the height anomaly at the center as suggested by the box in the middle of (a); the size of this anomaly is very small (≤50 μm, to be compared with the SPP's diameter of 8.4 mm). The small dots are blemishes not in the spiral phase plate but rather in the imaging system.

the beam has only propagated over a few wavelengths and thus has not had a chance to interfere with itself. A far-field intensity pattern, however, reveals all phase (and intensity) variations of the near field and enables us to probe the quality of the SPP.[9] Because of the chromaticity of the device, we expect that the vortex charge Q and therefore the far-field profiles will vary as a function of the wavelength of the input beam. Therefore we recorded far-field profiles for our SPP at different input wavelengths. Here, we used as a bright white-light source a femtosecond mode-locked Ti:sapphire laser (Coherent Vitesse) in combination with a microstructured fiber of 1-m length with a 1.7-μm core diameter (Crystal Fiber A/S).[24] The white light generated in the microstructured fiber was spatially filtered by use of a single-mode fiber (Newport F-SA; cutoff wavelength, 400 ± 50 nm) to produce a beam close to a fundamental Gaussian. Subsequently this beam

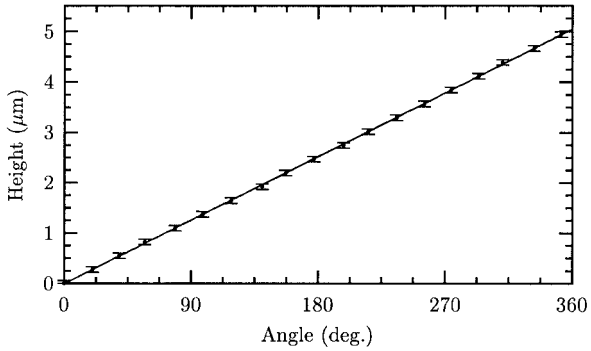

Fig. 6. The angular position of each dark fringe on the ramp as it occurs in Fig. 5(a) is measured, converted to a height, and plotted as a point here. The line shows a linear fit, demonstrating the excellent linearity of the ramp.

was spectrally filtered with a set of narrowband interference filters, each of which had a bandwidth of ≤10 nm. Thus we obtained a quasi-monochromatic Gaussian beam of variable wavelength with good spatial coherence with which to study the phase-modifying effects of the SPP. This beam was made to pass through the SPP, after which the far field of the resultant beam was imaged onto a CCD camera. The results are shown at the top of Fig. 7. As can be seen, the first two profiles [Fig. 7(a) and 7(b)], taken at wavelengths 540 and 674 nm, respectively, show zero-intensity spots lying close together, near the center, and one lying off center to the right, all caused by phase singularities.[9] The former correspond to the integer part of the topological charge of the field.

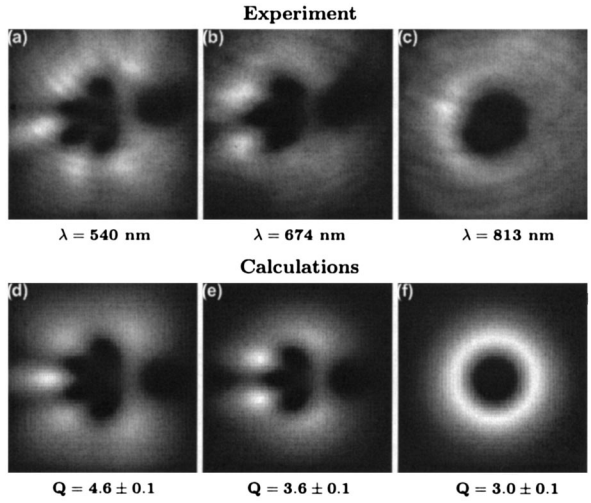

Fig. 7. Top, far-field diffraction patterns of fundamental Gaussian beams of different wavelengths that have passed through the spiral phase plate with its step oriented upward. Bottom, calculated far-field diffraction patterns with different values of Q. Black and white correspond to low and high intensities, respectively. For each of the calculated patterns the value of Q (given below the pattern) was adjusted to visually match the experimentally obtained diffraction patterns. The zero intensity spots near the center and those to the right in both the experimental and the calculated patterns correspond to phase singularities.

The latter, isolated phase singularity, which corresponds to the noninteger part of charge Q, has been pushed off center in the horizontal direction, a phenomenon that occurs as a result of the upward-oriented edge discontinuity in the near-field phase distribution.[25] The presence of this off-center intensity zero led us to conclude that, for these wavelengths (540 and 674 nm), the step height of the phase plate gives rise to an optical phase jump that is not a multiple of 2π. The diffraction pattern observed at 813 nm, as shown in Fig. 7(c), shows a reasonably nice doughnut shape and does not display an off-center isolated intensity zero. We can therefore conclude that, at this wavelength, the optical phase jump is almost exactly equal to $2\pi Q$, with Q an integer number.

To better assess the quality of our device we compared our results with calculated far-field patterns. To calculate these we modeled the input beam as a Gaussian amplitude and plane phase distribution and let this beam impinge upon an ideal (i.e., free of manufacturing constraints) SPP with vorticity Q. This ideal SPP was so thin that propagation aspects inside the device could be ignored. The output field was then Fourier transformed and to obtain the far field. For each wavelength used in the experiment we calculated such far-field intensity distributions, adjusting the value of Q to visually match the profile found in the experiment. The results are shown in Figs. 7(d)–7(f). We can conclude that the experimentally obtained images agree quite well with the calculations. The same experiment was repeated for a SPP produced in the same mold with a different polymer, yielding different vorticities. Also for this device, good agreement with the calculations was achieved. Calculations that took the angular width of the step into account revealed no fundamental changes in the structure of these far-field patterns, justifying the comparison of the experimental SPP device with an ideal SPP device.

It is well known that replicated optics can exhibit considerable (stress-induced) birefringence. To assess whether the SPPs replicated with this technology are birefringent, we inserted one such device into an optical beam between two crossed polarizers. Regardless of the orientation of the SPP in this setup, the intensity was measured to be less than 5×10^{-5} of the incident intensity. We thus concluded that our SPPs are highly polarization isotropic.

C. Reproducibility

A last point that we checked is the reproducibility of the molding process. The idea is to use a SPP to imprint a certain vorticity onto a fundamental Gaussian beam and, by employing a nominally identical SPP with the same orientation but with opposite vorticity, to correct the phase pattern created by the first, positive vorticity plate, thereby reconstructing the original beam. Thus, when the SPPs do not complement each other, the original beam is not reconstructed, as illustrated in Fig. 8. We easily obtained an opposite vorticity SPP by fabricating a second device from the same polymer in the same mold and then flipping it about the axis defined by the step, as shown in Fig. 9.

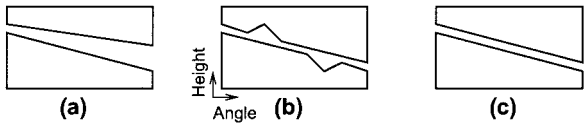

Fig. 8. Demonstration of ways in which one may detect errors in the structure of the phase plates by combining devices from the same mold in such a way that, ideally, the effects of the two devices cancel. (a) If reproducibility is bad, e.g., if each device shrinks differently during polymerization, the devices will not complement each other. (b) If the ramp of one device contains a flaw, the second device will also contain that flaw but at a different angular position. (c) Perfect devices and perfect reproducibility; the SPPs complement each other.

This procedure was implemented in the following experiment: A He–Ne laser beam was allowed to propagate through two of the previously specified SPPs (for which Q is a noninteger at $\lambda = 633$ nm), placed in each other's near fields with an $f - 2f - f$ telescope, as shown in Fig. 10. The resultant beam was then coupled into a single-mode fiber, which allowed only a fundamental Gaussian beam to propagate, and the output power was measured. Without the SPPs this power was measured to be 58% of the power emitted by the laser. With the SPPs present and after correction for reflection losses of the SPPs we found a value of 57% of the laser power. Natu-

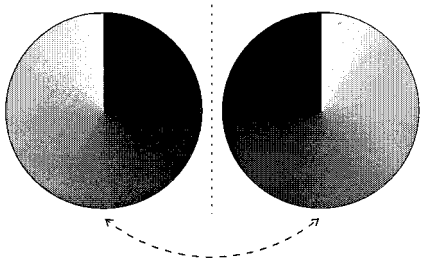

Fig. 9. Illustration of how to invert the vorticity of a SPP. The left-hand device, with a clockwise vorticity as indicated by the gray-scale gradient, is flipped by 180° about the vertical dotted line, which is parallel to the step. The result is the device at the right, with counterclockwise vorticity.

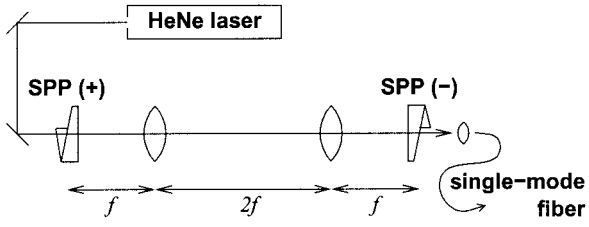

Fig. 10. A He–Ne beam is allowed to propagate through two nominally identical, opposite-vorticity SPPs, each placed in the other's near field. The output beam is coupled into a single-mode fiber. The beam intensity after the fiber is 98% of the intensity when no SPPs are inserted in the beam.

rally, the throughput is sensitive to precise alignment of the two SPPs. For instance, if one SPP was moved in the transverse direction over a distance of 10% of the width of the incident beam, the throughput was decreased by a factor of 2.

From the normalized transmission of 0.98, we concluded that the optical beam after the second SPP is Gaussian. This assumption was substantiated by measurements of the far-field profile.[26] If the SPP had not been reproducible, e.g., if each device were polymerized and shrunk differently, the transmission would not have been so high, as illustrated in Fig. 8(a). The normalized throughput value of 0.98 can be used as a quantitative measure of the replication process, implying that the mold is extremely well suited for reproducible production of SPPs.

This result also supports our claim that the phase pattern imprinted by the SPP deviates only a little from the ideal. That is, any flaw would occur in both SPPs at the same location. As one SPP is inverted by being flipped as shown in Fig. 9, the single flaw will occur at two different locations in the imprinted phase, as shown in Fig. 8(b). If then also the reproduction were inaccurate, as suggested by Fig. 8(a), the results in this experiment would be disastrous. The fact that the reconstructed beam has such a large overlap with the original incident Gaussian beam proves that the ramp is as smooth as it can be and that reproduction of the SPP is accurate; thus the quality of the devices is excellent, approaching that of ideal SPPs.

This experiment has also demonstrated that these SPPs are ideal for adding and subtracting vorticity from a field, thus providing the possibility of combining devices to generate lower-order optical vortices; a combination of two SPPs produced from the same mold, but made from polymers with slightly different refractive indices, can achieve exactly that.

5. Conclusions

We have described the production of a spiral phase plate with a smooth ramp that is capable of generating optical beams of low-order vorticity. We have discussed both the manufacture of the mold and the fabrication of the plate itself. We used several diagnostic methods to scrutinize the optical quality of the device and the smoothness of the surface, all of which led to the conclusion that the spiral phase plate produced is of very high quality. The replication process is excellent, producing identical plates with a modal accuracy of $>98\%$ in a first try. Additionally, it allows for production of devices with different vorticities from the same mold; the vorticity depends on the choice of polymer. It then becomes possible to combine several plates to achieve, in principle, any desired topological charge. We are confident that these plates can be used in the study of phase singularities and of the orbital angular momentum of classic light and that of single photons.

We are grateful to Mathijs de Jongh of Campus Technology Center of the Philips Enabling Technologies Group (Eindhoven, The Netherlands) for carefully crafting the molds. This work is part of the research program of the 'Stichting voor Fundamenteel Onderzoek der Materie' and is supported by the European Union program Active Teleportation and Entangled State Information Technology.

References

1. L. Allen, M. W. Beijersbergen, R. J. C. Spreeuw, and J. P. Woerdman, "Orbital angular momentum of light and the transformations of Laguerre–Gaussian laser modes," Phys. Rev. A **45,** 8185–8189 (1992).
2. A. T. O'Neill, I. MacVicar, L. Allen, and M. J. Padgett, "Intrinsic and extrinsic nature of the orbital angular momentum of a light beam," Phys. Rev. Lett. **88,** 053601 (2002).
3. A. Y. Bekshaev, M. V. Vasnetsov, V. G. Denisenko, and M. S. Soskin, "Transformation of the orbital angular momentum of a beam with optical vortex in an astigmatic optical system," JETP Lett. **75,** 127–130 (2002).
4. S. Kuppens, M. Rauner, M. Schiffer, K. Sengstock, W. Ertmer, F. E. van Dorsselaer, and G. Nienhuis, "Polarization-gradient cooling in a strong doughnut-mode dipole potential," Phys. Rev. A **58,** 3068–3078 (1998).
5. E. M. Wright, J. Arlt, and K. Dholakia, "Toroidal optical dipole traps for atomic Bose–Einstein condensates using Laguerre–Gaussian beams," Phys. Rev. A **63,** 013608 (2000).
6. H. He, M. E. J. Friese, N. R. Heckenberg, and H. Rubinsztein-Dunlop, "Direct observation of transfer of angular momentum to absorptive particles from a laser beam with a phase singularity," Phys. Rev. Lett. **75,** 826–829 (1995).
7. M. E. J. Friese, J. Enger, H. Rubinsztein-Dunlop, and N. R. Heckenberg, "Optical angular momentum transfer to trapped absorbing particles," Phys. Rev. A **54,** 1593–1596 (1996).
8. J. F. Nye, *Natural Focusing and Fine Structure of Light* (Institute of Physics, Bristol, UK, 1999).
9. M. W. Beijersbergen, R. P. C. Coerwinkel, M. Kristensen, and J. P. Woerdman, "Helical-wavefront laser beams produced with a spiral phaseplate," Opt. Commun. **112,** 321–327 (1994).
10. J. Arlt, K. Dholakia, L. Allen, and M. J. Padgett, "Parametric down-conversion for light beams possessing orbital angular momentum," Phys. Rev. A **59,** 3950–3952 (1999).
11. A. Mair, A. Vaziri, G. Weihs, and A. Zeilinger, "Entanglement of the orbital angular momentum states of photons," Nature **412,** 313–316 (2001).
12. S. Franke-Arnold, S. M. Barnett, M. J. Padgett, and L. Allen, "Two-photon entanglement of orbital angular momentum states," Phys. Rev. A **65,** 033823 (2002).
13. M. Padgett, J. Courtial, L. Allen, S. Franke-Arnold, and S. M. Barnett, "Entanglement of orbital angular momentum for the signal and idler beams in parametric downconversion," J. Mod. Opt. **49,** 777–785 (2002).
14. H. H. Arnaut and G. A. Barbosa, "Orbital and intrinsic angular momentum of single photons and entangled pairs of photons generated by parametric down-conversion," Phys. Rev. Lett. **85,** 286–289 (2000).
15. E. R. Eliel, S. M. Dutra, G. Nienhuis, and J. P. Woerdman, "Comment on 'Orbital and intrinsic angular momentum of single photons and entangled pairs of photons generated by parametric down-conversion," Phys. Rev. Lett. **86,** 5208 (2001).
16. H. H. Arnaut and G. A. Barbosa, "Reply: Arnaut and Barbosa," Phys. Rev. Lett. **86,** 5209 (2001).
17. V. Y. Bazhenov, M. S. Soskin, and M. V. Vasnetsov, "Screw dislocations in light wavefronts," J. Mod. Opt. **39,** 985–990 (1992).
18. I. Basistiy, V. Y. Bazhenov, M. S. Soskin, and M. V. Vasnetsov, "Optics of light beams with screw dislocations," Opt. Commun. **103,** 422–428 (1993).

19. I. Basistiy, M. S. Soskin, and M. V. Vasnetsov, "Optical wavefront dislocations and their properties," Opt. Commun. **119,** 604–612 (1995).
20. A. G. Peele, P. J. McMahon, D. Paterson, C. Q. Tran, A. P. Mancuso, K. A. Nugent, J. P. Hayes, E. Harvey, B. Lai, and I. McNulty, "Observation of an x-ray vortex," Opt. Lett. **27,** 1752–1754 (2002).
21. S. C. Tidwell, G. H. Kim, and W. D. Kimura, "Efficient radially polarized laser beam generation with a double interferometer," Appl. Opt. **32,** 5222–5229 (1993).
22. J. Andrea, "Mass-production of diffraction limited replicated objective lenses for compact-disc players," in *Micromachining of Elements with Optical and Other Submicrometer Dimensional and Surface Specifications*, M. Weck, ed., Proc. SPIE **803,** 3–7 (1987).
23. T. G. Gijsbers, "COLATH, a numerical controlled lathe for very high precision," Philips Tech. Rev. **39,** 229–244 (1980).
24. A. V. Husakou and J. Herrmann, "Supercontinuum generation of higher-order solitons by fission in photonic crystal fibers," Phys. Rev. Lett. **87,** 203901 (2001).
25. G. Indebetouw, "Optical vortices and their propagation," J. Mod. Opt. **40,** 73–87 (1993).
26. S. S. R. Oemrawsingh, E. R. Eliel, J. P. Woerdman, E. J. K. Verstegen, J. G. Kloosterboer, and G. W. 't Hooft, "Half-integral spiral phase plates for optical wavelengths," submitted to J. Opt. A.